



OPEN

## Spectroscopic characterization and in vitro studies of biological activity of bradykinin derivatives

Edyta Proniewicz<sup>1✉</sup>, Grzegorz Burnat<sup>2</sup>, Helena Domin<sup>2</sup>, Emilia Iłowska<sup>3</sup>, Adam Roman<sup>4</sup> & Adam Prahł<sup>3</sup>

Eleven multiple analogs of bradykinin—a peptide that is a natural ligand of B1 and B2 receptors but does not bind or activate the B1 receptor unless Arg<sup>9</sup> is removed from the sequence by the action of carboxypeptidase N—were synthesized. Their biological activity was examined on T-REx cell lines expressing B1 or B2 receptors using the intracellular IP1 assay. The mRNA expression of B1R and B2R in the lysate of tumor cell lines, e.g., U87-MG (human astrocytoma), SHP-77 (human small cell lung cancer), and H4 (human brain glioma), was determined. For five B1R antagonists, adsorption at the liquid/solid interface (Au nanoparticles (AuNPs) served as the solid surface) was discussed in terms of the vibrations of molecular fragments (structural factors) responsible for the biological properties of these analogs.

Bradykinin (BK) (Table 1) belongs to the kinin protein group and influences a wide range of physiological responses via two metabotropic G protein-coupled receptors (GPCRs) known as B1 (B1R) and B2 (B2R). B2Rs are constitutively expressed in most cell types, whereas B1Rs are present only in tissue inflammation<sup>1</sup>. Activation of B2R causes slow, sustained smooth muscle contraction, alteration of epithelial cell ion secretion, increased vascular permeability, increased mucosal secretion, release of cytokines from leukocytes, stimulation of sensory neurons, and production of eicosanoids from a variety of cell types<sup>2,3</sup>. BK has been linked with a variety of diseases, including chronic pain, sepsis, asthma, rheumatoid arthritis, pancreatitis, and several other inflammatory diseases. BK is also considered a growth factor involved in the development and progression of cancer<sup>4</sup>. However, the mechanism of the tumor growth-promoting effect of this kinin is still unknown. GPCRs can be blocked by GPCR antagonists, which effectively compete with native peptides. Therefore, GPCR antagonists are an effective chemotherapeutic and diagnostic strategy in drug development<sup>5,6</sup>. In this context, several studies continue to focus on the development of mutant analogs that have both much higher affinity and antagonistic properties and weaker agonistic properties of these receptors. Because of these properties, specifically modified analogs can effectively compete with the native peptide; when they bind preferentially to GPCRs, they block these receptors from acting. Since clinical studies have shown that the main actions of BK are B2R functions, most attempts to synthesize effective BK antagonists have focused on analogs known as B2 bradykinin antagonists<sup>7,8</sup>. The search for B1R antagonists is also important because B1Rs are potential targets for drug development in pain processes<sup>9</sup>.

Understanding the effects of replacing naturally occurring amino acids with unnatural ones on peptide structure is critical to explaining and determining the role of individual amino acids in the physiological effects of BK. In this context, a number of analogs have been developed<sup>8–18</sup>. For example, it was discovered that the substitution of the L-proline residue at position 7 (Pro<sup>7</sup>) with D-phenylalanine ([D-Phe<sup>7</sup>]BK) is the key structural change in the sequence BK that alters the steric position of the C-terminal dipeptide Phe<sup>8</sup>-Arg<sup>9</sup> and leads to antagonistic B2R activity<sup>8,10</sup>. The addition of a D-arginine at the N-terminus (D-Arg<sup>0</sup>) and the replacement of Pro<sup>3</sup> with L-hydroxyproline (Hyp) increased the potency of the antagonist D-Arg<sup>0</sup>[Hyp<sup>3</sup>,D-Phe<sup>7</sup>]BK<sup>10</sup>. Replacement of two L-Phe residues at positions 5 and 8 with an unnatural amino acid that alters aromaticity in the C-termini has been shown to result in a partial agonist [Thi<sup>5,8</sup>]BK<sup>11</sup>. The addition of conformational constraints to the structure by replacing Phe<sup>8</sup> with a piperidine-2-acetic acid (Pip) group results in a compound with increased potency in vitro and metabolic stability towards B1R<sup>13</sup>. Removal of the C-terminal Arg<sup>9</sup> significantly decreases affinity for B2R. Acylation of the N-terminus with various bulky alkyl groups consistently improves antagonistic potency

<sup>1</sup>Faculty of Foundry Engineering, AGH University of Science and Technology, 30-059 Krakow, Poland. <sup>2</sup>Maj Institute of Pharmacology, Polish Academy of Sciences, Department of Neurobiology, 12 Smętna Street, 31-343 Kraków, Poland. <sup>3</sup>Faculty of Chemistry, University of Gdansk, Wita Stwosza 63, 80-308 Gdansk, Poland. <sup>4</sup>Maj Institute of Pharmacology, Polish Academy of Sciences, Department of Brain Biochemistry, 12 Smętna Street, 31-343 Kraków, Poland. ✉email: proniewi@agh.edu.pl

Abbrev.	Peptides' sequence										
	0'	0	1	2	3	4	5	6	7	8	9
BK			Arg	Pro	Pro	Gly	Phe	Ser	Pro	Phe	Arg
BK1		Aaa	Arg	Pro	Pro	Gly	Phe	Ser	Pro	Phe	Arg
BK2		Aca	Arg	Pro	Pro	Gly	Phe	Ser	Pro	Phe	Arg
BK3		D-Arg	Arg	Pro	Hyp	Gly	Thi	Ser	D-Phe	L-Pip	Arg
BK4	Aaa	D-Arg	Arg	Pro	Hyp	Gly	Thi	Ser	D-Phe	L-Pip	Arg
BK5		D-Arg	Arg	Pro	Hyp	Gly	Thi	Ser	D-Phe	D-Pip	Arg
BK6	Aaa	D-Arg	Arg	Pro	Hyp	Gly	Thi	Ser	D-Phe	D-Pip	Arg
BK7	Aaa	D-Arg	Arg	Pro	Hyp	Gly	Thi	Ser	D-Phe	Thi	Arg
BK8		D-Arg	Arg	Pro	Hyp	Gly	Thi	Ser	L-Pip	Thi	Arg
BK9	Aaa	D-Arg	Arg	Pro	Hyp	Gly	Thi	Ser	L-Pip	Thi	Arg
BK10		D-Arg	Arg	Pro	Hyp	Gly	Thi	Ser	D-Pip	Thi	Arg
BK11	Aaa	D-Arg	Arg	Pro	Hyp	Gly	Thi	Ser	D-Pip	Thi	Arg

**Table 1.** Sequences of studied bradykinin analogs. Aaa—[(3 s,5 s,7 s)-adamantan-1-yl]acetic acid, Aca—(3 s,5 s,7 s)-adamantane-1-carboxylic acid, Thi – thienylalanine, Pip—piperidine-2-carboxylic acid, and Hyp—hydroxyproline.

in rat blood pressure assays<sup>12</sup>. Peptides with a suitable achiral, nonaromatic, conformationally bound amino acid, such as 1-aminocyclohexane-1-carboxylic acid (Acc) at position 7, can also have an antagonistic effect on B2R<sup>14,15</sup>. Substitution of five non-proteinogenic amino acids yields the BK analog icatibant ([D-Arg<sup>0</sup>,Hyp<sup>3</sup>,Thi<sup>5</sup>,D-Tic<sup>7</sup>,Oic<sup>8</sup>,desArg<sup>9</sup>]BK), which is a potent, specific and selective peptidomimetic B2R antagonist<sup>16</sup>. Icatibant has also been used to show that B1Rs increase in neuronal cells of STZ-diabetic rats. In pioneering work, D. Regoli and colleagues and F. Marceau also identified and characterized novel multimutated derivatives of [desArg<sup>9</sup>]BK that act as kinin B1 receptor agonists<sup>17,18</sup>.

Despite the great interest in BK and its antagonists, which are selective for a single receptor class and represent an extremely important tool for elucidating the physiological and pathological roles played by naturally occurring peptides and their receptors, there is still a great need for research on BK analogs with antagonistic properties. The studies presented in this paper are an integral part of this scientific problem and are devoted to several analogs of BK (Table 1) and the determination of their biological activity using cell lines overexpressing B1R and B2R, as well as the intracellular inositol monophosphate (IP1) assay.

The studies presented here also describe peptide structures and adsorption changes resulting from modifying the peptide chain. These issues need to be addressed to better understand the interaction mechanism between BK and the receptors and are critical for the development of new BK antagonists with increased affinity for the receptors. Surface-enhanced Raman scattering (SERS) has shown promise in structural-activity studies to predict the biochemical activity of some neuropeptides<sup>19–21</sup>. For example, SERS has been used to determine the adsorbed molecular structures and the changes in these structures and adsorption resulting from substitution of natural amino acids by synthetic amino acids of bombesin (BN) and its analogs deposited on the Ag surface<sup>19</sup>. In the BN fragments, the relative efficacy of inhibiting the binding of <sup>125</sup>I-[Tyr<sup>4</sup>]BN to rat pancreatic acini cells was correlated with the behavior of the amide binding on the Ag surface, whereas the contribution of structural components to the ability to interact with the GPCR was correlated with the SERS patterns. In other words, SERS enabled the identification of important amino acid residues involved in substrate-receptor interactions in systems where biological studies are difficult or do not clearly identify the molecular fragments responsible for the biological activity of the peptide.

SERS is a method for studying structure, molecular interactions, and conformational changes based on their vibrational fingerprint<sup>22</sup>. It uses highly concentrated fields in the vicinity of resonantly excited plasmonic structures to obtain a signal enhancement of 10<sup>3</sup> to 10<sup>10</sup> compared to the Raman signal<sup>23</sup>. In SERS, the energy of the incident radiation is very low and the risk of sample destruction or damage is low, so it can be successfully used to study biological material. SERS uses nanostructures of Ag<sup>24</sup>, Au<sup>25</sup>, and, less commonly, Cu<sup>26</sup>, or other metals<sup>27,28</sup>. Metal sols are the most biologically important nanostructures because they ensure low dispersion of nanoparticle diameter in the sol, do not require strict topological control, and provide strong enhancement that decreases dramatically with a continuous metal layer<sup>29</sup>. In humid air, Cu, Ag, and Au slowly corrode and darken to form a metal oxide layer. Corrosion of metals in the human body is always accompanied by a gradual and slow release of metal ions into the body<sup>30</sup>. Wataha et al. examined various Au alloys for the release of metal ions into the cell culture medium and found that Au ions generally do not dissolve in the medium, but Ag and Cu ions do<sup>31</sup>. For this reason, we chose colloidal Au for our study.

## Results and discussion

**Biological activity studies.** Mock cells without transfection of bradykinin receptors were first used for the functional assay. As shown in Fig. 1A, the T-REx 293 cell lines did not respond to various doses of BK in the IP1 assay. Next, a cell line expressing one of the BK receptors was analyzed. Cells were exposed to different doses of BK and the influence of the selected reference antagonists R 892 (B1R antagonist) and WIN 64338 (B2R antagonist) was checked (Fig. 1B,C). The T-REx 293/B1R cell line increased intracellular IP1 levels in a dose-dependent

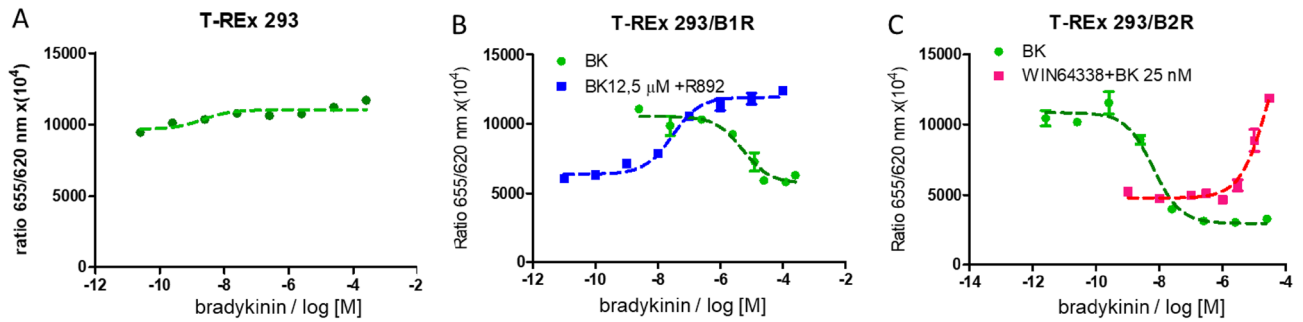


**Figure 1.** Influence of BK on IP1 levels in the mock T-REx 293 cell line. There is no functional activity of a BK receptor in this cell line because it is not expressed (A) and the effect of BK on T-REx 293 cells expressing B1R (B) or B2R (C). A dose-dependent increase in intracellular IP1 level was observed in presence of BK. In addition, specific antagonist activity for B1R and B2R was examined in the presence of BK, corresponding to EC<sub>80</sub> for each receptor (12.5  $\mu$ M for B1R and 25 nM for B2R).

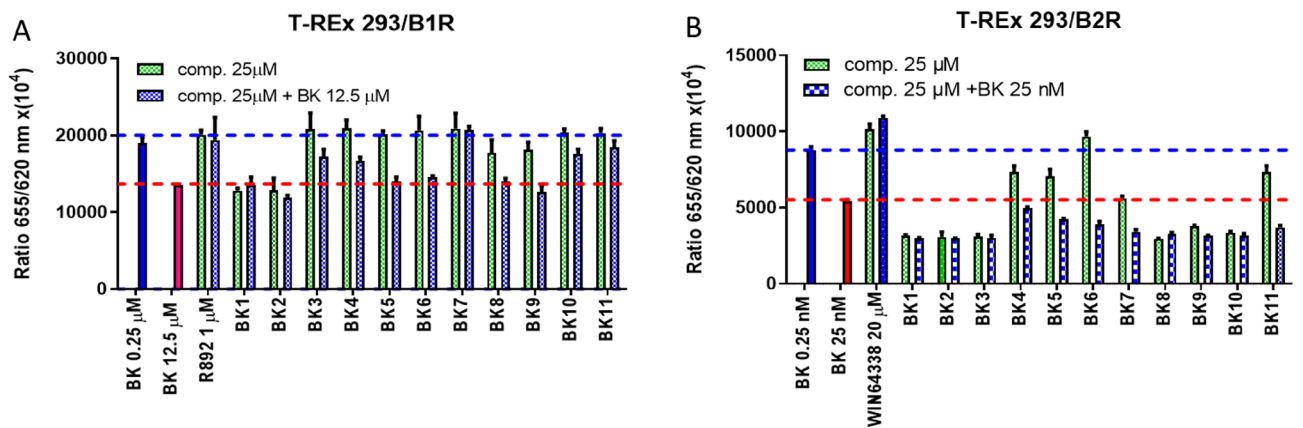


**Figure 2.** The activity of BK derivatives in the screening assay: (A) B1R and (B) B2R. The blue dashed line represents the lowest BK concentration that does not work, and the red line corresponds to the EC<sub>80</sub> value for a given receptor. Agonistic effects were examined by treating cells with the compounds alone (green bars) or with BK in EC<sub>80</sub> to examine their inhibitory effects (red bars).

manner. The half-maximal effective concentration (EC<sub>50</sub>) for B1R was calculated to be 1305 nM (SD  $\pm$  675 nM). The B1R antagonist R 892 decreased IP1 levels in a dose-dependent manner in the presence of concentration EC<sub>80</sub> BK (1250 nM). The EC<sub>50</sub> value for R 892 was calculated to be 69 nM (SD  $\pm$  66 nM) (Fig. 1B). The BK showed higher efficacy for B2R EC<sub>50</sub> 8 nM (SD  $\pm$  5 nM) in the T-REx 293 cell lines. The B2R antagonist WIN 64338 showed a dose-dependent inhibitory effect in the presence of BK 25 nM, corresponding to EC<sub>80</sub> (Fig. 1C).

Eleven derivatives of BK were analyzed in the screening procedure using both cell lines. The compounds were administered alone or in the presence of BK, corresponding to the EC<sub>80</sub> of the antagonist (Fig. 2). For B1R, compounds BK1 and BK2 showed agonistic activity alone (Fig. 2A). Compounds BK5/6/8 and BK9 were neutral to receptor activity but did not abolish bradykinin action. An antagonistic effect in the presence of BK was observed for compounds BK3/4/7/10 and BK11.

In screening experiments with the B2R cell line, compounds BK4, BK5, BK6, and BK11 showed a mild agonistic effect (Fig. 2B). The derivative BK6 has no agonistic effect, but also does not reverse the effect of BK. The agonistic effect was significantly stronger for compounds BK1/2/3/7/8/9 and BK10.

For all compounds that showed an antagonistic effect in the presence of bradykinin in the T-REx 293/B1R cell line, we attempted to determine the IC<sub>50</sub> in the concentration range  $2.5 \times 10^{-9}$ – $2.5 \times 10^{-4}$  M (Fig. 3). We succeeded in determining this parameter for compound BK11 (Fig. 3E), and it was 1186 nM (SD  $\pm$  817 nM). Other bradykinin derivatives were active only at the highest concentration between 25  $\mu$ M and 250  $\mu$ M, and the sigmoidal shape of the dose–response curve was not observed for these compounds because there was no saturation effect.

The expression of B1R and B2R was examined in some tumor cell lines, such as U87-MG, SHP-77, and H4 using a qRT-PCR method. As shown in Fig. 4, mRNA expression for both receptors was detected in all cell lines. B1R mRNA was greatest in the U87-MG cell line and lowest in the H4 cells. In general, the B2 receptor mRNA was lower compared with that of B1R. B2R mRNA was most abundant in SHP-77 and least abundant in the H4 cell line.

In further experiments, the U87-MG, SHP-77, and H4 cell lines were used for the functional assay with BK and the reference B1R antagonist. As shown in Fig. 13S in Supplementary File, all three cell lines expressed the functional B1R protein and its activity according to the mRNA level shown in Fig. 4. The obtained results are

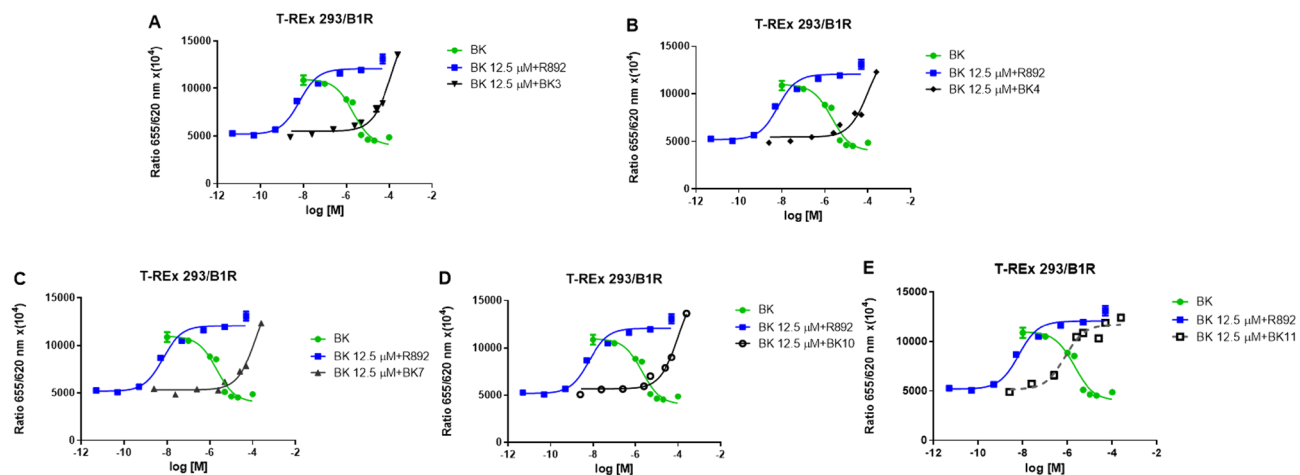


**Figure 3.** The pharmacodynamic effects of compounds showing inhibitory activity in the B1R screening assay. R892, the B1R antagonist, was used as the reference compound (blue line).

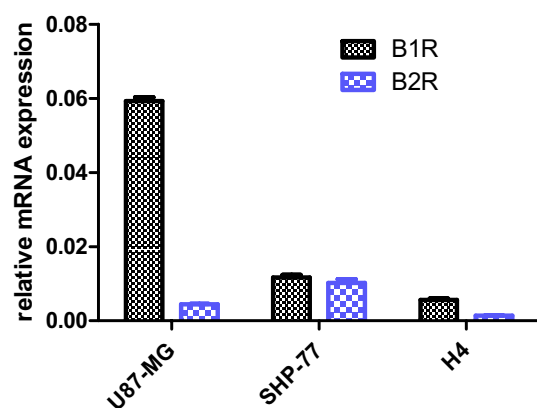


**Figure 4.** mRNA expression of B1R and B2R in the lysate of cancer cell lines: U87-MG, SHP-77, and H4.

consistent with previous findings showing the expression of functional B1R and B2R genes and proteins in human glioblastoma cells U87-MG<sup>32,33</sup>. In other studies, cellular expression of B1 and B2 receptors was detected in five different subtypes of human lung carcinomas (adenocarcinoma, squamous cell carcinoma, large cell carcinoma, small cell carcinoma, and carcinoid tumors)<sup>34</sup>. In addition, B2R has also been characterized in the cell line SHP-77<sup>35</sup>. However, to our knowledge, this is the first time that we have detected B1R and B2R gene expression in H4 cells of human brain neuroglioma and B1R in SHP-77 cells of human lung carcinoma. Interestingly, both U87-MG and H4 cell lines expressed higher levels of B1R mRNA compared with B2R, which could be explained by the inducible property of B1R under abnormal conditions, such as cancer<sup>36</sup>.

The cytotoxic potential of B1R antagonists such as BK3, BK4, BK7, BK10, and BK11 in H4, U87-MG, and SHP-77 cells was evaluated using the MTT assay, the most commonly used assay to evaluate the cytotoxic activity of the compounds. Cisplatin, a cytostatic drug commonly used for cancer chemotherapy, was used as a reference compound. Novel B1R antagonists exhibited varying levels of cytotoxic activity across cell lines and concentrations (Table 2). The obtained results indicate that the B1R derivatives studied may have anti-cancer properties in cell lines H4, U87-MG, and SHP-77.

To verify whether the cytotoxic effects of the new B1R antagonists are mediated by apoptosis, the activation level of caspase-3, a key enzyme in the apoptosis process, and PARP protein, the caspase-3 substrate, were determined by Western blot analysis.

Cisplatin at 25  $\mu$ M was used to induce control apoptosis. No significant change in the amount of cleaved PARP or caspase-3 activation was observed after B1R antagonist treatment compared with untreated cells (Fig. 5). These results suggest that the apoptotic caspase-3/PARP pathway is not involved in the cytotoxic activity of the B1R antagonists studied, which may be due to the low activity of the antagonists.

Our results are consistent with previous data showing that BK inhibitors can modulate cancer growth<sup>37,38</sup>, but to our knowledge, we have presented for the first time new results describing the cytotoxic effects of B1R antagonists in human brain neuroglioma cells H4 and human lung carcinoma cells SHP-77. We also found that B1R antagonists reduce the viability of glioma cells in human U87-MG glioblastoma astrocytoma cells. These

	H4	U87-MG	SHP-77
Control	99.999 ± 8.74	99.999 ± 5.246	100.000 ± 3.402
Cisplatin 25 µM	25.389 ± 3.71****	50.357 ± 4.97****	53.631 ± 12.052****
Cisplatin 100 µM	5.809 ± 1.488****	32.63 ± 6.934****	37.989 ± 11.626****
BK7 100 µM	97.73 ± 10.825	73.685 ± 12.815	86.685 ± 3.392
BK3 25 µM	83.049 ± 5.547	71.45 ± 7.763	87.804 ± 2.366
BK3 100 µM	70.937 ± 6.678	67.69 ± 6.873*	69.182 ± 5.170*
BK4 25 µM	74.075 ± 11.923	65.679 ± 5.21*	72.081 ± 5.974*
BK4 100 µM	50.773 ± 8.516***	59.113 ± 7.61***	52.663 ± 2.26****
BK10 25 µM	74.264 ± 11.923	79.495 ± 3.125	76.587 ± 5.974
BK10 100 µM	60.421 ± 3.769**	68.451 ± 4.128*	52.663 ± 2.26*
BK11 25 µM	94.235 ± 3.538	96.125 ± 1.241	96.421 ± 3.474
BK11 100 µM	65.668 ± 3.305*	81.07 ± 4.542	85.391 ± 5.646

**Table 2.** The effects of B1R antagonists (BK7, BK3, BK4, BK10, and BK11) and cisplatin on cancer cell lines (H4, U87-MG, and SHP-77) using MTT assay. Data were normalized to absorbance in the control group (100%) and are expressed as a percentage of control and presented as mean ± SEM obtained from  $n = 3$  wells per experiment from 2–3 independent experiments. \*\*\*\* $p < 0.0001$ ; \*\*\* $p < 0.001$ ; \*\* $p < 0.01$ ; \* $p < 0.05$  (one-tailed ANOVA and Tukey post hoc test).

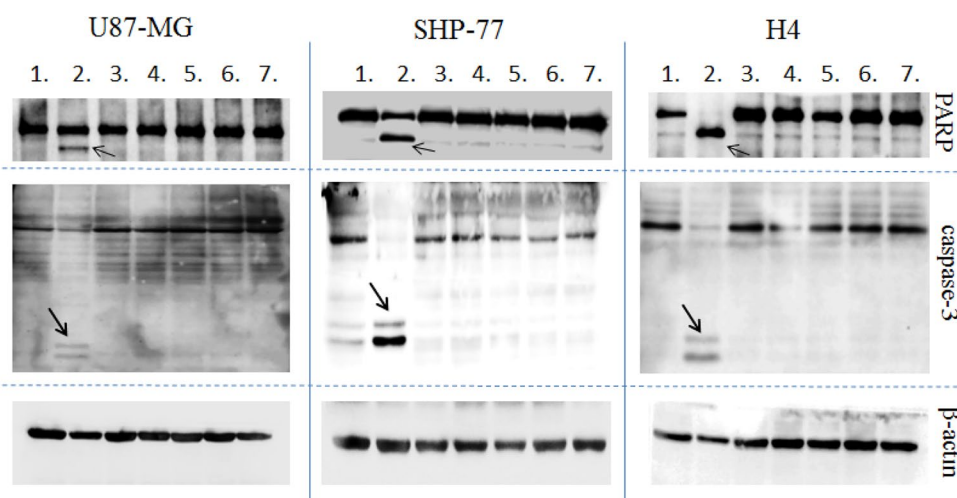


**Figure 5.** The effects of B1R antagonists and cisplatin on the expression levels of caspase-3 and PARP cleavage in cell lines U87-MG, SHP-77, and H4 were determined by Western blotting. **1.** control cells; **2.** cisplatin (25 µM); **3.** BK7 (50 µM); **4.** BK3 (50 µM); **5.** BK4 (50 µM); **6.** BK10 (50 µM); **7.** BK11 (50 µM). Arrows indicate the induction of caspase-3 and processed PARP fragments in cells treated with cisplatin as a positive control of apoptosis. After 24 h of cell treatment, no induction of caspase-3 and PARP is seen compared with untreated control cells. Representative Western blot images showing expression of  $\beta$ -actin were used as a reference protein. Each picture represents a vertically cut part of nitrocellulose membranes. The membranes were cut before antibody application, considering the size margin according to the size of the molecular weight marker.

results are in addition to previous literature evidence that B1R antagonists have cytotoxic effects on other glioblastoma cell lines such as U-138MG and U-251MG<sup>39</sup>.

**Analysis of SERS spectra.** Five of the eleven analogs of BK, i.e., BK3, BK4, BK7, BK10, and BK11, have antagonistic properties for B1R in the presence of bradykinin in the T-REx 293/B1R cell line ( $R892 >> BK11 > BK10 = BK7 = BK4 = BK3$ ), but none for B2R in the presence of bradykinin in the T-REx 293/BK2R cell line. Figure 6 shows the SERS spectra (solid lines) for these analogs adsorbed on the surface of AuNPs. This figure also includes the corresponding Raman spectra (dashed lines) to highlight the differences (in terms of band enhancement, wavenumber, and half-width at band maximum (fwhm)) between the SERS and Raman spectra, which are necessary to properly describe adsorption.

The antagonistic property of BK11 towards B1R in the presence of native BK is much stronger than for other analogs. Taking into account the common mutations in the structure of all five peptides (D-Arg<sup>0</sup>, Hyp<sup>3</sup>, and Thi<sup>5</sup>), it appears that the combination of modifications in the D-Pip<sup>7</sup> and Thi<sup>8</sup> positions with Aaa<sup>0</sup> produces an

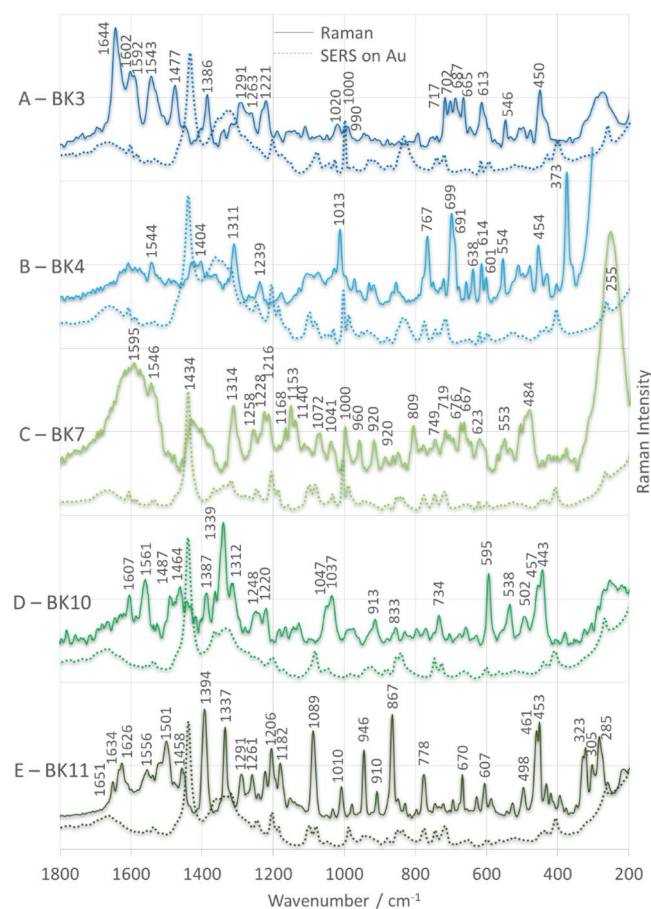


**Figure 6.** Raman (dashed line traces) and SERS (solid line traces) spectra of BK analogs adsorbed on AuNPs.

antagonistic effect. For this reason, the discussion focuses on the analysis of the spectra in terms of the vibrations of the molecular fragments (structural factors) responsible for the biological properties of these analogs.

Following the work of Fang et. al, who showed the results for piperidine adsorbed on the surface of colloidal Ag and an Ag electrode, the most intense SERS band at  $1394\text{ cm}^{-1}$  (fwhm =  $17\text{ cm}^{-1}$ ) (Fig. 6E) is due to vibrations of D-Pip<sup>7,40</sup>. Based on density functional theory calculations (DFT), they proposed that this band corresponds to the  $\rho_{\omega}(\text{CH}_2)$  mode of  $-\text{CH}_2-$  groups adjacent to the nitrogen atom. Based on the work of Selvaraj et al., the other two intense bands at  $1337\text{ cm}^{-1}$  (fwhm =  $12\text{ cm}^{-1}$ ) and  $1089\text{ cm}^{-1}$  (fwhm =  $15\text{ cm}^{-1}$ ) in the spectrum in Fig. 6E are assigned to the  $\nu(\text{C}-\text{C}) + \rho_{\omega}(\text{CH}_2) + \rho_{\text{b}}(\text{CH})$  and  $\rho_{\text{r}}(\text{CH}_2) + \rho_{\text{b}}(\text{CN}^-) + \rho_{\text{b}}(\text{CH}) + \rho_{\text{b}}(\text{ring})$  vibrations, respectively<sup>41</sup>. Knowing that (i) piperidine is saturated, which means that the only possible interaction of piperidine with the substrate surface is via its lone pair of electrons on the nitrogen atom, (ii) the selection rules of SERS state that the vibrations whose intensity comes from a large value of  $\alpha_{\text{zz}}$  (z is the local surface normal) are the most intense in the SERS spectrum, and (iii) the other intense vibrations observed in the SERS spectrum of BK11 are the in-plane skeletal stretching (at  $867\text{ cm}^{-1}$  (fwhm =  $12\text{ cm}^{-1}$ ) and  $1010\text{ cm}^{-1}$  (fwhm =  $10\text{ cm}^{-1}$ )) and the twisting vibrations (at  $946\text{ cm}^{-1}$  (fwhm =  $10\text{ cm}^{-1}$ ),  $1182$ , and  $1261\text{ cm}^{-1}$ )<sup>42</sup>, we can assume that piperidine is adsorbed in the end-on geometry with the N-containing molecular fragment interacting with the surface of the AuNPs.

We can expect similar bands to appear in the SERS spectrum of a BK10 analog (Fig. 6D) that contains D-Pip<sup>7</sup> in its sequence. In this peptide SERS spectrum, the band at  $1387\text{ cm}^{-1}$  is relatively weakly enhanced and broadened (fwhm =  $21\text{ cm}^{-1}$ ), whereas the band at  $1339\text{ cm}^{-1}$  (fwhm =  $17\text{ cm}^{-1}$ ) is the strongest in the spectrum ( $I_{1387}/I_{1339} = 0.6$  compared with  $I_{1394}/I_{1337} = 1.1$  for BK11). The other piperidine bands are absent or only weakly enhanced for BK11. Therefore, it can be assumed that the piperidine ring lies flat on the surface of the AuNPs. This can be confirmed by the bands at  $1037\text{ cm}^{-1}$  [ $\rho_{\omega}(\text{CH}_2) + \rho_{\text{ipb}}(\text{CH}) + \rho_{\text{b}}(\text{ring})$ ],  $1047\text{ cm}^{-1}$  [ $\rho_{\omega}(\text{CH}_2) + \rho_{\text{b}}(\text{ring})$ ],  $1317\text{ cm}^{-1}$  [ $\rho_{\omega}(\text{CH}_2)$ ], and  $1464\text{ cm}^{-1}$  [ $\rho_{\text{s}}(\text{CH}_2)$ ]<sup>20,41</sup>, which are more intense in the SERS spectrum of BK10 than in the SERS spectrum of BK11.

In the sequence of each peptide there is a Thi residue at position 5. The analogs BK7, BK10, and BK11 also contain Thi at position 8. The vibrations characteristic of the 2-substituted thiophene ring can be assigned to the bands at  $1501\text{ cm}^{-1}$  (fwhm =  $23\text{ cm}^{-1}$ ),  $1458\text{ cm}^{-1}$  (fwhm =  $18\text{ cm}^{-1}$ ),  $1206\text{ cm}^{-1}$  (fwhm =  $10\text{ cm}^{-1}$ ),  $670\text{ cm}^{-1}$  [ $\rho_{\text{oopb}}(\text{CH})$ , fwhm =  $8\text{ cm}^{-1}$ ],  $630\text{ cm}^{-1}$  [ $\rho_{\text{ipb}}(\text{ring}) + \nu(\text{C}-\text{S})$ , fwhm =  $9\text{ cm}^{-1}$ ],  $530\text{ cm}^{-1}$  [ring deformation +  $\rho_{\text{oopb}}(\text{CH})$ , fwhm =  $11\text{ cm}^{-1}$ ],  $498\text{ cm}^{-1}$  [ $\rho_{\text{ipb}}(\text{C}-\text{CH}_2)_{\text{subst}}$ , fwhm =  $12\text{ cm}^{-1}$ ],  $461\text{ cm}^{-1}$  (fwhm =  $9\text{ cm}^{-1}$ ), and  $453\text{ cm}^{-1}$  (fwhm =  $10\text{ cm}^{-1}$ ) in the BK11 SERS spectrum<sup>20,41,42</sup>. The SERS signals at  $1501$  and  $1458\text{ cm}^{-1}$  are due to the antisymmetric and symmetric  $\nu(\text{C}_{\alpha}=\text{C}_{\beta})$  modes, respectively, conjugated to  $\delta(\text{CH})$ <sup>43</sup>. A band at  $1206\text{ cm}^{-1}$  is assigned to the  $\nu(\text{C}_{\alpha}-\text{C}_{\alpha 2})$  ring mode<sup>44</sup>. The

bands at 461 and 453  $\text{cm}^{-1}$  are due to ring deformation (torsion) coupled to  $\rho_{\text{oopb}}(\text{CH})^{45}$ . All of these bands are smaller in intensity and width than the piperidine bands. However, two of them, at 1501 and 1206  $\text{cm}^{-1}$ , are the most intense vibrations of Thi and the bands with the fraction of C–S vibrations (at 747, 850, and 630  $\text{cm}^{-1}$ ) have the lowest intensity. It is also worth noting that  $\nu(\text{Ag–S})$ , which is expected in the wavenumber range of 180–250  $\text{cm}^{-1}$  when the adsorbate from the first monolayer interacts directly with the metal surface by charge transfer from the adsorbate to the metal or vice versa, is not present in the SERS spectrum of BK11<sup>46</sup>. According to the surface selection rule of Moskovits et al., the above results indicate a nearly horizontal orientation of the plane of the thiophene ring near the AuNP surface, which means that the molecule interacts only weakly via the sulfur atom.

In the SERS spectrum of BK10 analog (Fig. 6D), the Thi bands are generally less intense than the corresponding SERS signals for BK11, except for the bands at 502, 457, and 443  $\text{cm}^{-1}$ . In addition, the band at 538  $\text{cm}^{-1}$  is more intense and a new band appears at 595  $\text{cm}^{-1}$  [ $\rho_{\text{ipb}}(\text{ring}) + \nu(\text{C–S})$ ]. Also, in BK7 (Fig. 6C), most of the Thi bands decrease in intensity compared to BK11, while the SERS signals at 1501 and 1458  $\text{cm}^{-1}$  practically disappear, and the 255  $\text{cm}^{-1}$  spectral feature, which is due to  $\nu(\text{Au–N})$ , is the strongest band in the spectrum<sup>47</sup>. Moreover, in the low-energy region of the spectra (below 400  $\text{cm}^{-1}$ ), where the  $\nu(\text{Au–S})$  vibrations are expected, three bands of intermediate intensity appear only for BK11 at 323, 305, and 285  $\text{cm}^{-1}$ . Comparing the data from the literature, the above bands can be assigned to different types of Au–S bond vibrations, i.e., radial Au–S bond stretching at 285  $\text{cm}^{-1}$ , tangential Au–S bond stretching at 323  $\text{cm}^{-1}$ , and Au–S–C stretching at 305  $\text{cm}^{-1}$ <sup>48</sup>.

## Conclusions

Eleven bradykinin derivatives were synthesized and analyzed in a screening procedure using the T-REx 293/B1R and T-REx 293/B2R cell lines. Five of the eleven BK-analogs, including BK3, BK4, BK7, BK10, and BK11, have antagonistic properties for B1R in the presence of bradykinin in the T-REx 293/B1R cell line ( $\text{R892} > \text{BK11} > \text{BK10} = \text{BK7} = \text{BK4} = \text{BK3}$ ), but none show antagonistic properties for B2R in the presence of bradykinin in the T-REx 293/BK2R cell line. The cytotoxic/antiproliferative effects of these five analogs in cancer cell lines, such as H4, U87-MG, and SHP-77 were determined. The results showed that the B1R antagonists had varying degrees of cytotoxic effects depending on the cell lines and concentrations. This suggests that these analogs may have anticancer properties in cancer cell lines. Thus, our in vitro results suggest that B1R may be a promising target for cancer therapy. However, further data on the use of compounds with high B1R antagonist activity are needed to clarify the involvement of this receptor in anticancer strategies.

All five antagonists were immobilized at the AuNPs/liquid interface, and adsorption was monitored using SERS. The SERS spectra were analyzed in terms of the vibrations of these molecular fragments (amino acid side chains) responsible for the biological activity. Analysis of the SERS spectra shows that the combination of modifications at the D-Pip<sup>7</sup> and Thi<sup>8</sup> positions with Aaa<sup>0</sup> (the analog BK11) leads to a skeletal structure in which the piperidine ring adopts an end-on orientation with respect to the surface of the AuNPs. At this orientation, the nitrogen free electron pair is directed toward this surface, and the thiophene ring, whose free electron pair interacts only weakly with the AuNPs, assumes a nearly horizontal position relative to this surface. None of the other bradykinin analogs studied exhibits such an adsorbed structure, suggesting that the specific interaction between D-Pip<sup>7</sup> and Thi<sup>8</sup> and B1R, as well as the AuNP surface, may be responsible for the antagonistic properties of BK11.

## Methods

**Peptide synthesis.** Peptides were synthesized via the solid-phase method using the Fmoc/tBu strategy as previously described<sup>49</sup> with minor modifications and purified (see Supporting Information for details).

**Biological studies.** *Cell culture and transfection.* Cell lines overexpressing human B1R and B2R were prepared by transfection of the T-REx 293 cell lines (Thermo Fisher Scientific). This is a medicated HEK 293 (human embryonic kidney 293) cell line that allows the expression of the gene of interest in the pcDNA5/FTR/TO vector after the administration of tetracycline. The presence of tetracycline releases the Tet repressor protein (TetR) from the operon site and allows transcription of the mRNA (for details, see Supporting Information)<sup>50</sup>. The cancer cell lines, such as glioblastoma astrocytoma U87-MG and small cell lung carcinoma SHP-77 were purchased in ECACC. The brain neuroglioma cell line H4 was derived from ATCC.

*qRT-PCR.* The level of mRNA expression for B1R and B2R in the cancer cell lines was measured. Total RNA from the cells was extracted using TRIzol reagent (Thermo Fisher Scientific) according to the instructions (see Supporting Information for further details). The expression of each gene was quantified using the comparative threshold cycle method ( $\Delta\text{CT}$ ).

*Intracellular inositol monophosphate (IP-one) assay.* Receptor function was determined by measuring intracellular inositol monophosphate concentration using the IP-one kit from Cis-bio according to the procedure described previously (see Supporting Information for details)<sup>21</sup>. R 892 and WIN 64,338 hydrochloride (both from Tocris) were used as reference antagonists for B1R and B2R, respectively<sup>51</sup>.

*Cytotoxicity analysis.* The colorimetric tetrazolium salt assay with 3-(3,4-dimethylthiazol-2-yl)-2,5-diphenyltetrazolium bromide (MTT) was used to evaluate the cytotoxicity potential of the antagonists BK in the cancer cell lines H4, U87-MG, and SHP-77 (see Supporting Information for details)<sup>52</sup>.

**Western blot.** Western blot analysis was performed to evaluate the potential mechanism of cytotoxic activity of the antagonists of BK in cancer cell lines H4, U87-MG, and SHP-77 (see Supporting Information for details). Detection was performed using Pierce ECL Western blotting substrate (Thermo Fisher Scientific) and a Syngene GeneGnomeXRQ chemiluminescence analysis system. Primary antibodies:  $\beta$ -actin (1:10,000, Sigma, A5441), caspase-3 (1:1000, Cell Signaling, #9662S), poly(ADP-ribose) polymerase (PARP, 1:1000, Cell Signaling, #9532). Secondary antibodies: anti-rabbit (1:2500, Promega W401B) and anti-mouse (1:2500, Promega W402B).

**Colloids.** Three batches of colloidal Au solutions (20 nm,  $\sim 7.2 \times 10^{10}$  particles/mL, reactant-free, polydisperse index (PDI)  $< 0.2$ ,  $\lambda_{\max} = 529\text{--}533$  nm) were purchased from Merck (Poland).

**Raman and SERS measurements.** Spectra were acquired using an InVia Raman spectrometer (Renishaw) with a CCD detector and a Leica microscope (50 $\times$  objective). The spectral resolution was set to 4  $\text{cm}^{-1}$ . A diode laser with a wavelength of 785 nm (20 mW) served as the excitation source. The typical exposure time was 40 s with five accumulations. The SERS spectra of a given peptide were almost identical. No spectral changes were observed that could be associated with decomposition of the sample.

## Data availability

Data are available upon request (please contact the corresponding author: [proniewi@agh.edu.pl](mailto:proniewi@agh.edu.pl)).

Received: 16 July 2022; Accepted: 31 October 2022

Published online: 08 November 2022

## References

- Burch, R. M. Bradykinin receptors. In *Encyclopedia Biol. Chem.* (eds Lennarz, W. J. & Lane, M. D.), 240–243 (Academic Press, 2013).
- Sharma, J. N. & Al-Banoon, A. The role of inflammatory mediator bradykinin in cardiovascular and renal diseases. *Sci. Rep.* **1**, 142 (2012).
- Pirahanchi, Y. & Sharma, S. *Physiology* (StatPearls Publishing, 2021).
- Stewart, J. M., & Gera, L. Bradykinin and cancer. In *Handbook of Biologically Active Peptides* (ed. Kastin, A. J.), Chap. 63, 443–446 (Academic Press, 2006).
- Hauser, A. S., Attwood, M. M., Rask-Andersen, M., Schiöth, H. B. & Gloriam, D. E. Trends in GPCR drug discovery: New agents, targets and indications. *Nat. Rev. Drug Discov.* **16**, 829–842 (2017).
- Gutierrez, A. N. & McDonald, P. H. GPCRs: Emerging anti-cancer drug targets. *Cell Signal.* **41**, 65–74 (2018).
- Charignon, D., Spath, P., Martin, L. & Drouet, Ch. Icatibant, the bradykinin B2 receptor antagonist with target to the interconnected kinin systems. *Expert Opin. Pharmacother.* **13**, 2233–2247 (2012).
- Regolo, D., Allogho, S. N., Rizzi, A. & Gobeil, F. J. Bradykinin receptors and their antagonists. *Eur. J. Pharmacol.* **348**, 1–10 (1998).
- Talbot, S. *et al.* Cellular localization of kinin B1 receptor in the spinal cord of streptozotocin-diabetic rats with a fluorescent [Na-Bodipy]-des-Arg9-bradykinin. *J. Neuroinflamm.* **6**, 11 (2009).
- Vavrek, R. & Stewart, J. M. Competitive antagonists of bradykinin. *Peptides* **6**, 161–164 (1985).
- Śleszyńska, M. *et al.* New bradykinin B2 receptor antagonists - influence of C-terminal segment modifications on their pharmacological properties. *Acta Biochim. Pol.* **56**, 641–648 (2009).
- Sobolewski, D. & Prahl, A. Bradykinin analogues acylated on their N-terminus - some recent development. In *Peptides for Youth. Advances in Experimental Medicine and Biology* (eds Valle, S. D. *et al.*) (Springer, 2009).
- Fotsch, Ch. *et al.* A new class of bradykinin 1 receptor antagonists containing the piperidine acetic acid tetralin core. *Bioorg. Med. Chem. Lett.* **16**, 2071–2075 (2006).
- Labudda-Dawidowska, O. *et al.* New bradykinin analogues modified in the C-terminal part with sterically restricted 1-aminocyclohexane-1-carboxylic acid. *J. Med. Chem.* **48**, 8055–8059 (2005).
- Labudda, O. *et al.* New bradykinin analogues substituted in positions 7 and 8 with sterically restricted 1-aminocyclopentane-1-carboxylic acid. *J. Peptide Sci.* **12**, 775–779 (2006).
- Regoli, D., & Marceau, F. B-2 Bradykinin Receptor. *xPharm: The Comprehensive Pharmacology Reference*, 1–14 (2007).
- Marceau, F. Kinin B1 receptors: A review. *Immunopharmacol.* **30**, 1–26 (1995).
- Regoli, D., Neugebauer, W. A., Gobeil, F., Gabra, B., Sirois, P. Novel selective bradykinin (BK) B1 peptidic receptor antagonists and uses thereof, Patent number: 20040198666, October 7, (2004).
- Podstawka, E. Effect of amino acids modifications on non-adsorbed and adsorbed on electrochemically roughened silver surface molecular structure of bombesin 6–14 fragments. *J. Raman Spectrosc.* **39**, 1290–1305 (2008).
- Skoluba, D., Sobolewski, D., Prahl, A. & Proniewicz, E. Interaction of bradykinin and B2 bradykinin receptor antagonists with colloidal Au surface explored by surface-enhanced Raman scattering. *J. Spectrosc.* **2014**, 1–8 (2014).
- Proniewicz, E. *et al.* Application of alanine-scanning to determination amino acids essential for peptide adsorption at the solid/solution interface and binding to the receptor: SERS/SEIRA vs. bioactivity assays. *J. Med. Chem.* **64**, 8410–8422 (2021).
- Smith, E. W., Rodger, C., Dent, G., & White, P. C. Raman and surface enhanced resonance Raman scattering: applications in forensic science. In *Handbook of Raman Spectroscopy: From the Research Laboratory to the Process Line* (eds Lewis, I. R. & Edwards, H.), Chap. 18, 733–748 (CRC Press, 2001).
- Perez-Jimenez, A. I., Lyu, D., Lu, Z., Liu, G. & Ren, B. Surface-enhanced Raman spectroscopy: Benefits, trade-offs and future developments. *Chem. Sci.* **11**, 4563–4577 (2020).
- Piergies, N. *et al.* Fourier transform infrared and Raman and surface-enhanced Raman spectroscopy studies of a novel group of boron analogues of aminophosphonic acids. *J. Phys. Chem. A* **116**, 10004–10014 (2012).
- Domin, H. *et al.* SERS characterization of neuropeptide Y and its C-terminal fragments onto colloidal gold nanoparticles surface. *Coll. Surf. B* **149**, 80–88 (2017).
- Proniewicz, E. & Olszewski, T. SERS/TERS characterization of new potential therapeutics: influence of positional isomerism, interface type, oxidation state of copper and incubation time on adsorption on the surface of copper(I) and (II) oxide nanoparticles. *J. Med. Chem.* **65**, 4387–4400 (2022).
- Proniewicz, E. *et al.* Is the electrochemical or the green chemistry method the optimal method for the synthesis of ZnO nanoparticles for applications to biological material? Characterization and SERS on ZnO. *Coll. Surf. A* **609**, 125771 (2021).
- Proniewicz, E. *et al.* Electrochemically synthesized  $\gamma$ -Fe<sub>2</sub>O<sub>3</sub> nanoparticles as peptide carriers and sensitive and reproducible SERS biosensors. Comparison of adsorption on Fe<sub>2</sub>O<sub>3</sub> versus Fe. *App. Surf. Sci.* **495**, 143578 (2019).
- Tolstoy, V. P., Chernyshova, I. & Skryshevsky, V. A. *Handbook of Infrared Spectroscopy of Ultrathin Films* (Wiley, 2003).



30. Lygre, H. Prosthodontic biomaterials and adverse reactions: A critical review of the clinical and research literature. *Acta Odontol. Scand* **60**, 1–9 (2002).
31. Wataha, J., Craig, R. C. & Hanks, C. T. The release of elements of dental casting alloys into cell-culture medium. *J. Dental Res.* **70**, 1014–1018 (1991).
32. Pillat, M. M. *et al.* Glioblastoma-mesenchymal stem cell communication modulates expression patterns of kinin receptors: Possible involvement of bradykinin in information flow. *Cytom. A* **89**, 365–375 (2016).
33. Sun, D. P., Lee, Y. W., Chen, J. T., Lin, Y. W. & Chen, R. M. The bradykinin-BDKRB1 axis regulates aquaporin 4 gene expression and consequential migration and invasion of malignant glioblastoma cells via a Ca<sup>2+</sup>-MEK1-ERK1/2-NF- $\kappa$ B mechanism. *Cancers (Basel)* **12**, 667 (2020).
34. Chee, J., Naran, A., Misso, N. L., Thompson, P. J. & Bhoola, K. D. Expression of tissue and plasma kallikreins and kinin B1 and B2 receptors in lung cancer. *Biol. Chem.* **389**, 1225–1233 (2008).
35. Bironaite, D., Gera, L. & Stewart, J. M. Characterization of the B2 receptor and activity of BK analogs in SHP-77 cell line by Cytosensor microphysiometer. *Chem. Biol. Interact.* **150**, 283–293 (2004).
36. Lau, J., Rousseau, J., Kwon, D., Bénard, F. & Lin, K. S. A systematic review of molecular imaging agents targeting bradykinin B1 and B2 receptors. *Pharmaceuticals* **13**, 199 (2020).
37. Dubuc, C. *et al.* Antitumor activity of cell-penetrant kinin B1 receptor antagonists in human triple-negative breast cancer cells. *J. Cell Physiol.* **234**, 2851–2865 (2019).
38. Wang, Y. *et al.* Novel bradykinin receptor inhibitors inhibit proliferation and promote the apoptosis of hepatocellular carcinoma cells by inhibiting the ERK pathway. *Molecules* **26**, 3915 (2021).
39. Nicoletti, N. F. *et al.* Mechanisms involved in kinin-induced glioma cells proliferation: The role of ERK1/2 and PI3K/Akt pathways. *J. Neurooncol.* **120**, 235–244 (2014).
40. Hao, Y. & Fang, Y. Piperidine adsorption on two different silver electrodes: A combined surface enhanced Raman spectroscopy and density functional theory study. *J. Nanopart. Res.* **9**, 817–824 (2007).
41. Selvaraja, S., Rajkumara, P., Kesavanb, M., Gunasekaranc, S. & Kumaresan, S. Experimental and theoretical analyzes on structural and spectroscopic properties of monomer and dimeric form of (S)-Piperidine-2-Carboxylic acid: An attempt on medicinal plant. *Vib. Spectrosc.* **100**, 30–39 (2019).
42. Świąch, D. *et al.* Tip-enhanced Raman spectroscopy of bradykinin and its B<sub>2</sub> receptor antagonists onto colloidal suspended Ag nanowires. *Phys. Chem. Chem. Phys.* **17**, 22882–22892 (2015).
43. Pasterny, K., Wrzalik, R., Kupka, T. & Pasterna, G. Theoretical and experimental vibrational studies on liquid thiophene and its acetonitrile solution. *J. Mol. Struct.* **614**, 297–304 (2002).
44. Chen, F., Zhang, J., Fu, M. & Shi, G. Raman spectroscopic studies on the structural changes of poly(3-methylthiophene) during heating and cooling processes. *Chin. Sci. Bull.* **47**, 1791–1793 (2002).
45. Singh, D. K., Srivastava, S. K., Ojha, A. K. & Asthana, B. P. Vibrational study of thiophene and its solvation in two polar solvents, DMSO and methanol by Raman spectroscopy combined with ab initio and DFT calculations. *J. Mol. Struct.* **892**, 384–391 (2008).
46. Nyamekye, Ch. K. A., Weibel, S. C. & Smith, E. A. Directional Raman scattering spectra of metal–sulfur bonds at smooth gold and silver substrates. *J. Raman Spectrosc.* **52**, 1246–1255 (2021).
47. Zhao, S., Tian, X. Z., Liu, J. N., Ren, Y. L. & Wang, J. J. Density functional study of molecular nitrogen adsorption on gold-copper and gold-silver binary clusters. *J. Mol. Model.* **20**, 2467 (2014).
48. Bürgi, T. Properties of the gold–sulfur interface: From self-assembled monolayers to clusters. *Nanoscale* **7**, 15553–15567 (2015).
49. Proniewicz, E., Maluch, I., Kudelski, A. & Prah, A. Adsorption of (Phe-h5)/(Phe-d5)-substituted peptides from neurotensin family on the nanostructured surfaces of Ag and Cu: SERS studies. *Spectrochim. Acta A* **242**, 118748 (2020).
50. Das, A. T., Tenenbaum, L. & Berkhout, B. Tet-on systems for doxycycline-inducible gene expression. *Curr. Gene Ther.* **16**, 156–167 (2016).
51. Gobeil, F. Jr. *et al.* Kinin B1 receptor antagonists containing alpha-methyl-L-phenylalanine: In vitro and in vivo antagonistic activities. *Hypertension* **33**, 823–829 (1999).
52. Domin, H., Jantas, D. & Śmiałowska, M. Neuroprotective effects of the allosteric agonist of metabotropic glutamate receptor 7 AMN082 on oxygen-glucose deprivation- and kainate-induced neuronal cell death. *Neurochem. Int.* **88**, 110–123 (2015).

## Acknowledgements

This work was supported by the National Science Centre in Poland (grant no. 2016/21/B/ST4/02135 to E.P.), AGH University (subsidy no.: 16.16.170.654), and statutory funds from the Maj Institute of Pharmacology, Polish Academy of Sciences, Krakow, Poland.

## Author contributions

E.P.: funding of the research, research concept and design, RS and SERS measurements, data analysis, drawing figures and writing the original manuscript, discussion with reviewers, and final version of the manuscript; E.I. and A.P.: chemical synthesis and analysis of peptides; G.B. and H.D.: biological activity studies, data analysis, participation in drawing figures and writing the original manuscript; participated in discussion with reviewers and revision of the final version of the manuscript; A.R.: participation in the biological activity studies. All authors approved the final version of the manuscript.

## Competing interests

The authors declare no competing interests.

## Additional information

**Supplementary Information** The online version contains supplementary material available at <https://doi.org/10.1038/s41598-022-23448-7>.

**Correspondence** and requests for materials should be addressed to E.P.

**Reprints and permissions information** is available at [www.nature.com/reprints](http://www.nature.com/reprints).

**Publisher's note** Springer Nature remains neutral with regard to jurisdictional claims in published maps and institutional affiliations.



**Open Access** This article is licensed under a Creative Commons Attribution 4.0 International License, which permits use, sharing, adaptation, distribution and reproduction in any medium or format, as long as you give appropriate credit to the original author(s) and the source, provide a link to the Creative Commons licence, and indicate if changes were made. The images or other third party material in this article are included in the article's Creative Commons licence, unless indicated otherwise in a credit line to the material. If material is not included in the article's Creative Commons licence and your intended use is not permitted by statutory regulation or exceeds the permitted use, you will need to obtain permission directly from the copyright holder. To view a copy of this licence, visit <http://creativecommons.org/licenses/by/4.0/>.

© The Author(s) 2022